Evaluation of the Electron Temperature of the Ablation Cloud for the Small-Size Hydrogen Pellet Using Paschen Series in Heliotron J

Akihiro IWATA, Shinichiro KADO[1)], Gen MOTOJIMA[2)], Taiichi SHIKAMA[3)], Minato MURAKUMO[3)], Atsuki MORI, Hiroyuki OKADA[1)], Takashi MINAMI[1)], Shinsuke OHSHIMA[1)], Shigeru INAGAKI[1)], Fumiyoshi KIN[1)], Shinji KOBAYASHI[1)], Akihiro ISHIZAWA, Yuji NAKAMURA, Shigeru KONOSHIMA[1)], Tohru MIZUUCHI[1)] and Kazunobu NAGASAKI[1)]

Graduate School of Energy Science, Kyoto University, Uji 611-0011, Japan
[1)]*Institute of Advanced Energy, Kyoto University, Uji 611-0011, Japan*
[2)]*National Institute for Fusion Science, Toki 509-5292, Japan*
[3)]*Graduate School of Engineering, Kyoto University, Kyoto 615-8530, Japan*

(Received 4 September 2023 / Accepted 16 February 2024)

We simultaneously measured the electron temperature (T_e) and electron density (n_e) using a low-dispersion near-infrared spectrometer in a small-size pellet ablation cloud in Heliotron J, a medium-sized helical-axis heliotron device. We applied the intensity ratio of the Paschen-α, β, and γ to determine T_e based on the collisional-radiative model, which was fairly consistent with the partial local thermodynamic equilibrium (LTE) in the upper principal quantum numbers of 4, 5, and 6. For a typical pellet injection discharge, T_e and n_e were determined to be 0.9 eV and 4×10^{21} m^{-3}, respectively. Our derived generalized empirical calibration curve demonstrates a weak influence of T_e on n_e evaluation, particularly in the range of 0.4 - 2.0 eV. Subsequently, we determined the region where the LTE is achieved for the Paschen series.

Keywords: pellet ablation cloud, near-infrared spectroscopy, collisional-radiative model, partial LTE, electron temperature measurement, Heliotron J

DOI: 10.1585/pfr.19.1402017

1. Introduction

The injection of the hydrogen ice pellet is one of the most important methods for fueling fusion plasma. The physics of pellet ablation must be clarified to develop the optimal fueling scenario. The neutral gas shielding (NGS) [1] and neutral gas and plasma shielding (NGPS) [2] models have been proposed to predict pellet ablation behavior and are being compared with observations of pellet trajectories and lifetimes based on strong Balmer-α emissions from the ablation cloud. However, for a more quantitative comparison between models and observations, it is desirable to measure the plasma parameters used in these models, namely the electron temperature (T_e) and the electron density (n_e).

The Stark broadening of the hydrogen atomic spectrum emitted from the ablation cloud was used to measure n_e in the cloud in LHD [3], and the intensity of the radiative continuum spectrum was employed to evaluate T_e. In that case, the n_e of the ablation cloud was determined to be of the order of 10^{23} m^{-3} through the Stark broadening of the Balmer-β (H_β, 486.135 nm) in the visible (VIS) region. Simultaneously, T_e was estimated to be approximately 1 eV [4]. However, when the pellet is small and, consequently, the n_e value in the cloud is relatively low ($\sim 10^{21}$ m^{-3}) [5], the intensity of the radiative continuum spectrum is also low. Thus, it becomes difficult to evaluate T_e. In our previous work, the Paschen-α (Pa_α, 1875.13 nm) line in the near-infrared (NIR) region, which has a wider Stark width than H_β, was used to measure the lower n_e value in the Heliotron J [6]. The Stark width has a strong dependence on n_e; however, it also demonstrates a weak dependence on T_e. In Ref. [6], the plasmoid of the ablation cloud was assumed to be in the local thermodynamic equilibrium (LTE) state. Hence, the T_e value was set to 1 eV, which is typically valid for LTE plasma. Although the Stark broadening of the atomic hydrogen line emission from the ablation cloud is highly dependent on n_e, its value can be modified by T_e. Therefore, it is important to evaluate the range of T_e and its effect on the n_e measurement.

In this study, instead of using the radiative continuum spectrum, we measure the intensity ratio of the Paschen-α, β and γ to determine T_e based on the collisional-radiative model, using a simple low-dispersion NIR spectrometer. This measurement can be taken simultaneously with the Stark broadening measurement reported in Ref. [6]. Sub-

author's e-mail: iwata.akihiro.73c@st.kyoto-u.ac.jp

sequently, we assess the parameters at which we can assume (at least partially) the local thermal equilibrium in determining T_e. Finally, we discuss the population balance in the ablation cloud.

2. Experimental Setup

Pellet injection experiments were conducted in Heliotron J, a medium-sized helical-axis heliotron device. The pellet injection system and the NIR spectroscopy system were installed in the # 11.5 port, as shown in Fig. 1. The pellet injection system produces a cylindrical solid hydrogen pellet with a diameter of 0.7 mm and ejects it at a speed of approximately 250 m/s. In the NIR spectroscopy system, the emission from the pellet ablation cloud is focused by the objective lens (THORLABS F220SMA-A, a collimator lens with a focal length of f = 10.92 mm, numerical aperture NA = 0.25) and then transmitted to the spectrometer (Ocean Optics, Inc., NIRQuest 512-2.2) via a 16-m long low-OH fiber (THORLABS FT400EMT, a core diameter of 400 μm and a NA value of 0.39). The spot diameter of the sight line is approximately 12 mm at the plasma center. The spectrometer is a compact and low-dispersion crossed Czerny-Turner-type spectrometer equipped with a thermoelectrically cooled (−20°C) InGaAs linear sensor (Hamamatsu G9206-512W, 512 channels, pixel dimension of 10 × 250 μm^2, horizontal pixel pitch of 15 μm, sensitivity range of 800 - 2150 nm), a grating of 100 lines/mm, and a 100-μm slit without a long-pass filter that absorbs light in the visible region. The measurement range is approximately 905 - 2140 nm, and the reciprocal linear dispersion is 96.49 nm/mm at the center of the detector. Note that the second and even the third-order diffraction light may overlap in the NIR region when the emission line has high intensity. The absolute sensitivity calibration of the spectrometer was performed using a tungsten-halogen lamp (USHIO, JC100V500W) as a standard light source, cutting the second-order diffracted light from the visible region (525 - 800 nm) using an external 1050 nm long-pass filter [7].

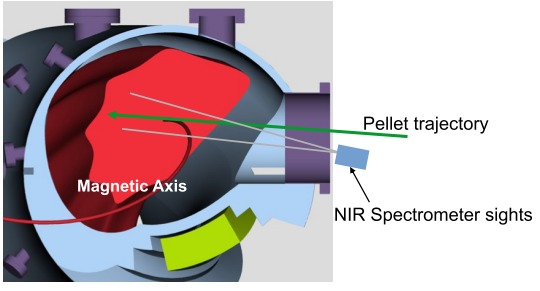

Fig. 1 Cross section at the # 11.5 port in Heliotron J. The pellet injection system and the NIR spectroscopy system were installed in this port.

3. Results

Figure 2 shows the temporal evolution of the monitoring parameters (Shot # 75847). Deuterium plasma in a low-toroidicity magnetic field configuration was generated through electron cyclotron resonance heating (ECH) and maintained via neutral beam injection (NBI). In this discharge, the pellet was injected at 244 ms in the NBI phase. Then, the plasma underwent radiative collapse. The intensity of H_α peaked at the pellet injection, and a fringe jump occurred in the line-averaged electron density. We also monitored the impurity lines with monochromators (Nikon P-250) that had a wavelength resolution of 0.06 nm and a wavelength accuracy of 0.3 nm. The impurity oxygen OV ($1s^2 2s 3s\,^3S - 1s^2 2s 3p\,^3P^o$; 278.1 nm) intensity increased after pellet injection and then rapidly decreased with W_p, indicating plasma cooling during the radiation collapse. The carbon CIII ($1s^2 2s 3s\,^3S - 1s^2 2s 3p\,^3P^o$; 464.7 nm) intensity increased to an over-range value, indicating the presence of low T_e plasma below the ionization barrier.

The exposure time for NIR spectroscopy was set to 10 ms, which included the pellet injection time. Therefore, the obtained signal reflects the brightest spectrum in time and space of the observation. Figure 3 shows the NIR spectra in shot #75847 without the visible light cut-off filter. Pa_α, Pa_β, Pa_γ, and the second and third-order spectra of H_α were observed. The electron density determined from the Stark broadening of Pa_α, 1.5±0.3 nm was (4±1)×10^{21} m^{-3} when T_e = 1 eV was assumed.

In the evaluation of T_e, we applied the collisional-radiative (CR) model for neutral hydrogen [8, 9]. This

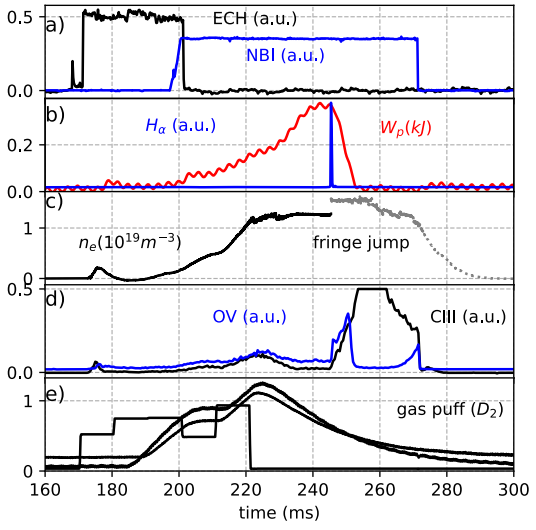

Fig. 2 Time evolution of the target plasma (Shot #75847). The pellet was injected at 244 ms in the NBI phase. a) Heating via ECH and NBI. b) H_α intensity at the #11.5 port (H_α) and the plasma stored energy (W_p). c) The line-averaged electron density (n_e). The fringe jump occurred at the moment when the pellet was injected. d) Beryllium-like oxygen (OV) and carbon (CIII). e) Gas puff signal of deuterium.

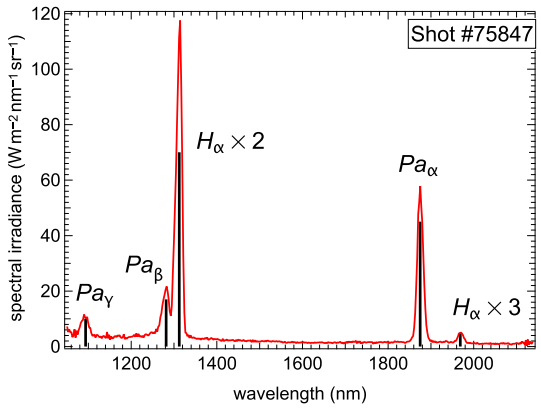

Fig. 3 NIR calibrated spectra in shot #75847. Pa$_\alpha$, Pa$_\beta$, Pa$_\gamma$, and the second and third-order spectra of H$_\alpha$ were measured.

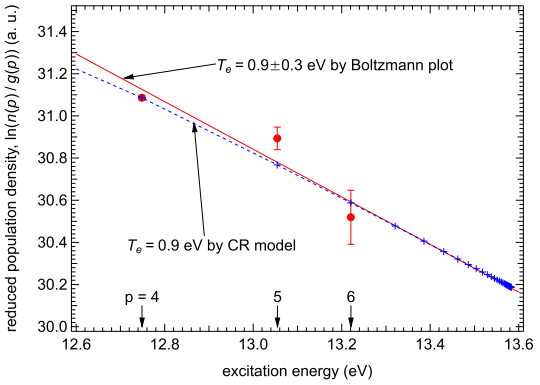

Fig. 4 Reduced population densities of the Paschen series measured in shot #75847. The upper level p is shown on the excitation energy axis. The blue cross points represent CR model results under the conditions of $n_e = 4 \times 10^{21}$ m^{-3}, and $T_e = 0.9$ eV. The red solid line denotes the linear Boltzmann plot. The electron temperature was determined to be 0.9 ± 0.3 eV from its slope.

model considers various atomic processes at each excitation level of a neutral hydrogen atom in the rate equation, and the steady-state solution gives the population density $n(p)$ at the excitation level p as:

$$n(p) = R_0(p)n_e n_i + R_1(p)n_e n(1) + R_2(p)n_e n_{\mathrm{H}_2}. \quad (1)$$

R_0, R_1, and R_2 are referred to as the population coefficients and are functions of n_e and T_e. n_i represents the ion density, $n(1)$ is the ground state atomic density, and n_{H_2} is the molecular density. Note that the last term in Eq. (1) is ignored here, because the formation of molecular H_2 is not considered in the pellet ablation process. For atomic hydrogen without considering the fine structure, p can be interpreted as the principal quantum number. Therefore, the upper states of the Paschen-α, β, and γ correspond to $p = 4$, 5, and 6, respectively.

The line intensities of the Paschen series were obtained via fitting with a Voigt profile. Subsequently, the populations per degeneracy, i.e., the reduced population densities, were plotted against the excitation energy, as shown in Fig. 4. In calculating the CR model under the conditions of $n_e = 4 \times 10^{21}$ m^{-3} and $T_e = 0.9$ eV, the relative intensities of the calculated results for levels $p = 4$, 5, and 6 best matched the experimental results. In such a pellet ablation process, the recombining component was dominant. Here, $n(1)$ is assumed to be 1×10^{21} m^{-3}, which is of the same order as n_e, as deduced from the Saha-Boltzmann equation for $n_e = 4 \times 10^{21}$ m^{-3} and $T_e = 0.9$ eV. In actuality, $n(1)$ has no effect on the recombining component and little effect on the line ratio for the ionizing component. We confirmed that the sensitivity of this assumption is sufficiently low. The reduced population densities obtained from the CR model calculations form approximately a straight line from the high excitation levels, indicating the establishment of a partial LTE (pLTE) state for levels above $p = 4$ under these electron density and temperature conditions.

In the LTE state, the reduced population densities and the excitation energies have the proportional relationship expressed in Eq. (2):

$$\frac{n(p)}{g(p)} \propto \exp\left(-\frac{E(p)}{k_B T}\right), \quad (2)$$

where $n(p)$, $g(p)$, and $E(p)$ are the population density, degeneracy, and excitation energy, respectively. k_B is the Boltzmann constant, and T is the electron temperature. Through the linear fitting of the semi-logarithmic plot, known as the Boltzmann plot (BP), the electron temperature $T_e\_BP(p = 4\text{ - }6)$ was determined to be 0.9 ± 0.3 eV from the reciprocal of its slope.

To evaluate the levels at which the LTE state can be considered valid, we evaluated the Griem's boundary, p_G, for hydrogen using Eq. (3) [10]. This boundary represents the lower limit above which the LTE approximation is valid.

$$p_G \simeq 1.6 \times 10^3 / n_e^{2/15}. \quad (3)$$

To assess the practically applicable boundary of BP, we calculated $T_e\_BP(p-1, p)$ from the slope between each adjacent pair of levels in the CR model results using Eq. (4).

$$T_e\_BP(p-1, p) = -\frac{E(p-1) - E(p)}{\ln\left[\frac{n(p-1)}{g(p-1)}\right] - \ln\left[\frac{n(p)}{g(p)}\right]}. \quad (4)$$

We calculated the reduced population densities under the conditions of $n_e = 4 \times 10^{21}$ m^{-3} and $n_e = 1 \times 10^{20}$ m^{-3} at $T_e = 0.9$ eV using the CR model, as shown in Fig. 5 (a). Figure 5 (b) shows the $T_e\_BP(p-1, p)$ evaluated using these results. For $p \geq 4$, which is higher than $p_G \sim 2.1$ at $n_e = 4 \times 10^{21}$ m^{-3}, the $T_e\_BP(p-1, p)$ was approximately 0.9 eV. $p = 4$ seems to be marginal for the LTE treatment in this condition. If n_e is lower, p_G increases, and the threshold level of the LTE state may be higher. The p_G value for $n_e = 1 \times 10^{20}$ m^{-3}, which falls below

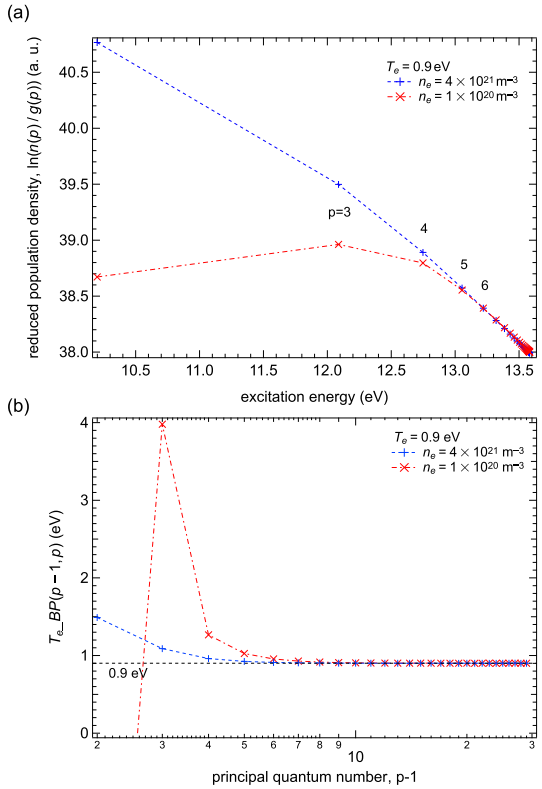

Fig. 5 (a) Reduced population densities of the CR model calculation and (b) T_e evaluated from the adjacent level, p and $p-1$ (T_e_$BP(p-1,p)$) using Eq. (4) in cases where $n_e = 4\times10^{21}$ m^{-3} and $n_e = 1\times10^{20}$ m^{-3} at $T_e = 0.9$ eV.

the lower limit of the ablation cloud density, was approximately 3.4. As shown in Fig. 5 (b), the deviation of the evaluated temperature from 0.9 eV increases as the levels become lower. The reduced population densities corresponding to lower levels in Fig. 5 (a) deviate from the straight line of the 0.9 eV Boltzmann temperature. Figure 5 (b) suggests that levels $p \geq 4$ for the density of the ablation cloud can be treated as pLTE, whereas the lower density violates the pLTE assumption. This can be confirmed by the slope, i.e., T_e_BP, between p = 3 - 4 and 4 - 5 in Fig. 5 (a). In these cases, the CR model needs to be applied. A comparison of the CR model and BP (p = 4 - 5) may confirm the validity of $p = 4$ as a marginal level. Although, the effect on the density measurement is sufficiently small, the results of the Boltzmann plots and the CR model calculations are consistent, suggesting that the observed pellet ablation plasma was in a pLTE state above $p = 4$. In low n_e cases, the population is inverted at $p = 2$. However, one does not need to consider this as long as using a Paschen series, i.e., $p - 1 \geq 3$.

4. Discussion

In this section, we discuss the sensitivity of the n_e determination to the T_e value. Then, a strategy for determining T_e is proposed, depending on the T_e region.

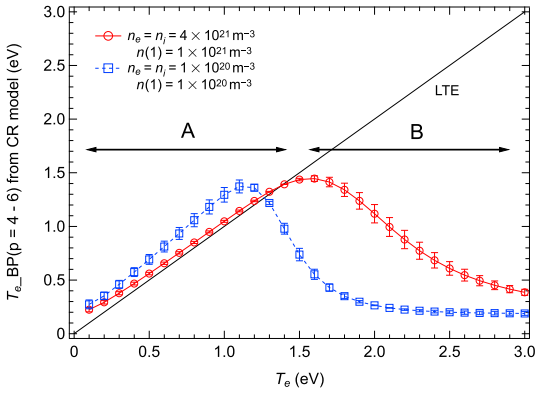

Fig. 6 Electron temperature from the Boltzmann plot for levels p = 4 - 6 (T_e_$BP(p$ = 4 - 6)) from the CR model in the range of 0.1 - 3.0 eV. The red circle represents the case of $n_e = 4\times10^{21}$ m^{-3}, and the blue square represents the case of $n_e = 1\times10^{20}$ m^{-3}. The black solid line denotes the electron temperature assuming LTE.

4.1 Influence of T_e on the n_e evaluation

As done in ref [6] for the fixed T_e of 1 eV, we deduced the n_e calibration curves for different values of T_e. Then, we obtained the generalized empirical calibration curve equation in the range of 0.4 - 2.0 eV as:

$$n_e \simeq (2.44 - 0.0791 T_e)\times10^{21}\times Stark\,width^{1.48}. \quad (5)$$

The T_e dependence is apparently weak in this T_e range, with a variation of approximately 5 % over this T_e range. This means that the effect is not severe, suggesting that knowing only the approximate value of T_e is sufficient. Particularly when the LTE approximation is valid, the interpretation of the phenomenon is straightforward. This condition will be satisfied when one measures the integrated spectra over time and space, following the methodology presented in this work.

However, if the population distribution deviates from LTE, we should be careful in determining T_e, particularly when only a limited number of lines can be obtained. This situation occurs when one tracks the spatial and temporal behavior of the ablation cloud because the ablation cloud is homogenized into a high-temperature bulk plasma. Considering these facts, the categorization of the T_e range is discussed.

4.2 LTE-like region

We examine the T_e range where the pLTE state is valid. We calculated $n(p)/g(p)$ from the CR model for a given T_e value in two cases: $n_e = 1\times10^{20}$ m^{-3} and $n_e = 4\times10^{21}$ m^{-3}, representing two typical scenarios. Then, T_e_BP was evaluated from p = 4 - 6 using the Boltzmann plot. For pLTE, we can expect $T_e = T_e$_BP. Figure 6 shows the electron temperature from the Boltzmann plot for p = 4, 5, and 6 (T_e_$BP(p$ = 4 - 6)) from the CR model results in the electron temperature range of 0.1 - 3.0 eV. In

this calculation, we assumed $n_e = n_i$, $n(1) = 1 \times 10^{20}\,\mathrm{m}^{-3}$, and $n(1) = 1 \times 10^{21}\,\mathrm{m}^{-3}$ for each n_e. In the range of 0.4 to 1.4 eV at $n_e = 4 \times 10^{21}\,\mathrm{m}^{-3}$ and for that of 0.4 to 1.3 eV at $n_e = 1 \times 10^{20}\,\mathrm{m}^{-3}$, the T_e_$BP(p = 4 - 6)$ values from the CR model are almost consistent with the straight line, assuming that these levels are in the LTE state. We refer to this region and the lower region (region A) as the LTE-like region. We refer to the temperature region higher than the LTE-like region (region B) as the higher-T_e region.

In the LTE-like region, T_e is determined using the Boltzmann plot for $p = 4 - 6$ (T_e_$BP(p = 4 - 6)$). Subsequently, we create a calibration curve at the determined T_e and evaluate n_e. For higher n_e, LTE must be established for $p = 4 - 6$. However, for lower n_e, $p = 4$ may gradually stop satisfying the LTE assumption, suggesting that more accurate T_e values can be obtained by using only $p = 5$ and 6. In this case, a visible light cut-off filter is needed to measure Pa_β without the influence of the second-order diffraction of H_α.

4.3 Higher-T_e region

In the higher-T_e region, the ionizing component is dominant. In this case, pLTE will not be satisfied anymore, meaning that the slope of the BP cannot reflect the T_e. Therefore, we can obtain the best fit T_e (T_e_CR) by comparing the relative intensities of the spectra with the results of the CR model calculated with n_e evaluated from the Stark width. This procedure can be repeated with new T_e values until the values converge.

Figure 6 shows that the slope exhibits an inverse dependence on T_e in the ranges of 1.5 eV to 3.0 eV (in cases where $n_e = 4 \times 10^{21}\,\mathrm{m}^{-3}$) and 1.4 eV to 2.5 eV (in cases where $n_e = 1 \times 10^{20}\,\mathrm{m}^{-3}$). Thus, fitting the CR model to the emission line intensity ratios may lead to multiple solutions for T_e. Note that when the number of measurable spectral lines is limited to a few, particularly when including marginal levels, such as $p = 4$, it is difficult to verify that the CR model's best fit temperature T_e_CR indicates T_e. Figure 6 shows that under the condition of a fixed electron density, the slope of BP can give two values of T_e for $T_e \geq 1.5$ eV.

In this case, we should determine whether the population satisfies LTE, depending on whether T_e is higher than the critical temperature between regions A and B.

5. Conclusion

To enhance the reliability of the n_e and T_e measurements in the ablation cloud formed by relatively small-size hydrogen ice pellets, T_e was evaluated using the relative intensities of the Paschen series spectra in the Heliotron J. From observation, we evaluated $T_e \sim 0.9$ eV, which is consistent with the assumed value in the previous work [6]. The CR model calculation indicates that the plasmoid of the ablation cloud is in the LTE state, even if the n_e is low (T_e = 0.4 - 1.4 eV for $n_e = 4 \times 10^{21}\,\mathrm{m}^{-3}$ and T_e = 0.4 - 1.3 eV for $n_e = 1 \times 10^{20}\,\mathrm{m}^{-3}$).

Regarding the influence of T_e on the determination of n_e, we derived and established the generalized empirical calibration curve equation over the range of 0.4 - 2.0 eV, showing a weak dependence of n_e on T_e ($\sim 5\%$ variation over this range). This suggests that T_e does not significantly impact the n_e evaluation.

For ablation cloud plasmas formed by the injection of small-size pellets, T_e can be determined by using the Boltzmann plot, which is a simple analysis that assumes LTE. Subsequently, n_e can be evaluated from the Stark broadening of Pa_α in the LTE-like region. However, as the ablation progresses and the cloud homogenizes into a high-temperature bulk plasma, we should be careful in determining T_e. An investigation into the spatiotemporal behavior of the ablation cloud is left for future work.

Acknowledgments

The authors are grateful to the staff of Heliotron J for performing the experiment. This work was supported by the NIFS Collaborative Research Program (Grant Nos. NIFS10KUHL030 and NIFS16KUHL073) and the JSPS Core-to-Core Program, A. Advanced Research Networks, "PLADyS".

[1] P.B. Parks and R.J. Turnbull, Phys. Fluids **21**, 1735 (1978).
[2] W. Houlberg *et al*., Nucl. Fusion **28**, 595 (1988).
[3] M. Goto *et al*., Plasma Phys. Control. Fusion **49**, 1163 (2007).
[4] G. Motojima *et al*., Rev. Sci. Instrum. **83**, 093506 (2012).
[5] G. Motojima *et al*., Plasma Phys. Control. Fusion **61**, 075014 (2019).
[6] A. Iwata *et al*., Rev. Sci. Instrum. **93**, 113537 (2022).
[7] S. Kado *et al*., Rev. Sci. Instrum. **89**, 10D129 (2018).
[8] K. Sawada and T. Fujimoto, J. Appl. Phys. **78**, 2913 (1995).
[9] T. Fujimoto *et al*., J. Appl. Phys. **66**, 2315 (1989).
[10] T. Fujimoto, *Plasma Spectroscopy* (Oxford University Press, USA, 2004).